

The effect of rubber particle size on toughening behaviour of rubber-modified poly(methyl methacrylate) with different test methods

Kilwon Cho*, JaeHo Yang and Chan Eon Park

Department of Chemical Engineering, Pohang University of Science and Technology,
790-784 Pohang, Korea

(Received 10 February 1997; revised 22 April 1997; accepted 19 August 1997)

In order to study the effect of particle size on the toughening behaviour of rubber-toughened poly(methyl methacrylate) (PMMA), a systematic model study has been carried out using core-shell type particles, made up of a poly(*n*-butyl acrylate) (PBA) core and a PMMA outer shell. Two different fracture tests, *i.e.* a three-point bending test for the evaluation of the fracture toughness (K_{IC}) and an impact test were employed to study the toughening behaviour. In the case of the impact test, maximum impact strength was obtained for rubber particles with a 0.25 μm diameter regardless of the rubber phase contents, and only a modest improvement of the impact strength was obtained for blends containing 0.15 or 2 μm particles. For the three-point bending test, in contrast, even large particles such as the 2 μm particles provided a significant enhancement in the fracture toughness. The difference in the toughening behaviour due to particle size may be attributed to the test method dependence associated with a change in the deformation mechanism. In the three-point bending test, the deformation mechanism was found to be multiple crazing, whereas in the impact test, the shear yielding induced by cavitation of the rubber particles is predominant. © 1998 Elsevier Science Ltd. All rights reserved.

(Keywords: poly(methyl methacrylate); toughening behaviour; particle size)

INTRODUCTION

It is well known that poly(methyl methacrylate) (PMMA) can be toughened by the addition of rubbery particles. The deformation and fracture behaviour of rubber-toughened PMMA has been the subject of much study^{1–11}. Although many studies have been reported on the mechanical behaviour of rubber-toughened PMMA, the deformation mechanism for rubber-toughened PMMA is still ambiguous, and contradictory results have been reported. PMMA itself is deformed mainly by crazing^{12–14}, but the deformation mechanism of rubber-toughened PMMA is influenced by the strain rate, the specimen geometry and the test method. Different deformation mechanisms, *i.e.* shear yielding^{1,2,4} and crazing^{3,6,9}, have been proposed according to the different test methods. Therefore, the deformation of rubber-toughened PMMA may possibly show different behaviour as the test conditions are changed.

The effect of the rubber phase fraction on the toughening behaviour is still unclear. Some authors have reported that the fracture toughness (K_{IC}) showed a sharp transition from brittle to ductile with increasing rubber phase content⁷, and others have found that the K_{IC} values increased monotonically with rubber content to a maximum value and then decreased with further increase of the rubber phase fraction⁸. With respect to the effect of the particle size, the optimum particle size for maximum toughness of rubber-toughened PMMA is known to be around 0.3 μm ^{1,2,10,15}. However, the reason for the existence of an optimum particle size has not yet been clearly explained.

The objective of this paper is to clarify the effect of the rubber particle size on the toughening behaviour of rubber-toughened PMMA under different fracture test methods, *i.e.* the impact test and the three-point bending test. For this purpose, a systematic model study has been carried out using core-shell type particles, which are made up of a poly(*n*-butyl acrylate) (PBA) core and a PMMA outer shell with a uniform particle size and composition. The fracture surfaces and the deformation region were observed by using various microscopy techniques. The deformation mechanism is also discussed in connection with the test method.

EXPERIMENTAL

Materials

The matrix PMMA resin was obtained from the Sumitomo Chemical Company (Sumpex-B MHO-G). The methyl methacrylate (MMA) and *n*-butyl acrylate (BA) monomers were used after removal of inhibitors by washing in 10 wt.% aqueous NaOH solution. Potassium persulfate (KPS), azobisisobutyronitrile (AIBN) and sodium dodecylsulfate (SDS) were used as received. 1,4-Butanediol diacrylate (BDA) and 1,4-butanediol dimethacrylate (BDMA) were used as cross-linking agents for the PBA rubbery core and the PMMA shell material, respectively.

Particle preparation

Core-shell particles were prepared by seeded emulsion polymerization. The rubbery core consisting of PBA was slightly cross-linked with BDA in order to maintain its shape and size during melt blending with matrix PMMA and

* To whom correspondence should be addressed. Tel.: +82-562-279-2270; fax: +82-562-279-2699; e-mail: kwcho@vision.postech.ac.kr

subsequent molding of the blends. The PBA core particles of the desired size (0.15–10 μm in diameter) were prepared by seeded emulsion polymerization in which seed particles were first formed and sequentially grown to the desired size. Emulsion polymerization was carried out in a round-bottomed glass reactor equipped with a reflux condenser, a glass stirrer, a nitrogen inlet tube, and a feeding tube which was connected to a syringe operated by a metering pump for controlling the feed rate.

The recipes for the preparation of the core particles are given in *Table 1*. For the preparation of the first PBA latex (#1 latex in *Table 1*), the materials of the pre-emulsion charge in *Table 1* were mixed at room temperature under a nitrogen atmosphere with mechanical agitation in order to form a monomer-in-water emulsion, which was termed the pre-emulsion. An aqueous KPS solution was added to the reactor heated to 80°C. The pre-emulsion was fed into the reactor during 6 h at a constant rate, and was then reacted for 2 h. In order to prepare large-size particles, seeded emulsion polymerization was employed. Water and the seed latex were charged into the reactor and heated to 80°C. The seed particles were sequentially grown to the desired size, *i.e.* the #1 latex was used as the seed latex for the preparation of the #2 latex, and then the #2 latex was used for the #3 latex, and so on. The pre-emulsion was fed into the reactor for 6 h at a constant rate and further reacted for 2 h. In order to prepare large-size particles by seeded emulsion polymerization, AIBN was used as initiator

instead of KPS because particles with a diameter greater than 1 μm cannot be prepared by using KPS¹⁶.

A typical procedure for the preparation of the PMMA shell is as follows. A 250 g amount of seed latex containing 100 g of solid PBA and 250 g of distilled water were charged into the reactor and heated to 80°C. The pre-emulsion was prepared from 150 g of MMA, 0.75 g of BDA, 1.71 g of AIBN, and 0.75 g of SDS in 220 g of water under vigorous agitation. The pre-emulsion was fed into the reactor at a constant rate for 4 h and further reacted for 2 h.

After preparation, the latex was coagulated, filtered and washed. The separated particles were dried in a vacuum oven at 60°C for 72 h. The dried particles were ground to a fine powder in a shredding mill. The morphology of the resulting particles was examined by scanning electron microscopy (SEM). Typical SEM micrographs of core-shell particles are shown in *Figure 1* for rubbery core sizes of 0.25 μm and 2 μm , displaying their uniform shapes and sizes. The sizes of the resulting particles were measured on the SEM micrograph and the size of the rubbery core was calculated. The diameter of the core particles prepared is given in *Table 1*. The glass transition temperature (T_g) of the core particles measured by dynamic mechanical testing was about -40°C .

Blending and specimen preparation

The core-shell particles were blended with PMMA pellets in a Brabender internal mixer at 180°C for 10 min. The

Table 1 Recipe for the preparation of core particles

Ingredient	Latex					
	#1	#2	#3	#4	#5	#6
Reactor charge (g)						
Water	150	140	60	20	20	200
Seed latex	–	17.5	40	70	120	210
KPS	0.54	–	–	–	–	–
Pre-emulsion charge (g)						
BA	108	125	98	100	110	120
BDA	1.08	1.25	0.98	1.0	1.1	0.6
Water	54	150	150	130	120	180
SDS	1.08	1.25	0.98	1.2	1.3	0.6
AIBN	–	1.4	1.3	1.2	1.1	1.4
Core particle diameter (μm)	0.15	0.25	0.8	2.0	6.2	9.7

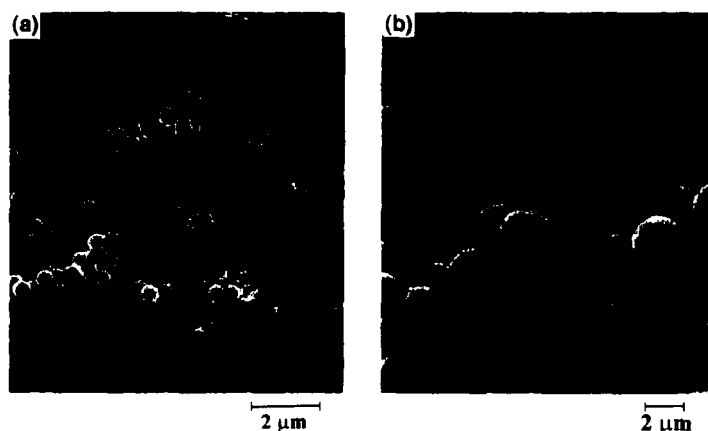


Figure 1 SEM micrographs of core-shell particles. Core particle size: (a) 0.25 μm ; (b) 2 μm

rubber-phase contents were varied from 5 to 20 wt.%. In the calculation of the rubber phase contents, the PMMA outer shell of the particles was also considered as a matrix component. The blends were compression-molded into 5 mm thick plates. The molded plates were machined into Charpy impact bars ($12.6 \times 5 \times 120 \text{ mm}^3$) and three-point bend specimens ($5 \times 10 \times 50 \text{ mm}^3$).

Mechanical tests

The fracture toughness (K_{IC}) was determined using a single-edge notched specimen by the three-point bending test (ASTM E399). A notch was machined into each specimen, which was precracked by the careful tapping of a fresh razor blade chilled in liquid nitrogen. At least six specimens were employed in a single determination of K_{IC} under each test condition. The tests were performed at room temperature at a cross-head speed of 1.28 mm min^{-1} using a universal test machine (Instron 4206). The Charpy impact strength was determined using a single-edge notched specimen (notch radius, 0.25 mm) at room temperature.

Microscopy

The fracture surfaces of the specimens broken by both the three-point bending and the impact tests were subjected to scanning electron microscopy (SEM; Hitachi S-570). Specimens were coated with a thin layer of gold-palladium. In order to examine the deformed region around the crack tip, a double-notched four-point bending test was performed and the deformed region around the unfractured notch tip of the four-point bending specimen was examined by transmission electron microscopy (TEM). The fracture subsurface of the impact test specimen was also examined by TEM. For the latter, the deformed zone was cut out from the specimen and stained with osmium tetroxide followed by ultramicrotomy, and was then examined by use of the Hitachi H-300 transmission electron microscope.

The fracture subsurfaces of the three-point bending test specimen and impact test specimen were examined by transmission optical microscopy (TOM). The well-established polishing/sectioning technique^{18,19} was employed. For this purpose, a section thin enough to transmit light was produced using the petrographic polishing technique. The fracture subsurfaces of the impact test, four-point bending test and three-point bending test specimens were examined under a bright field image using a Zeiss optical microscope. All samples examined were from the middle part of specimen, which satisfies the plane strain constraints.

RESULTS

Effect of particle size and rubber phase content on impact strength

The impact strength is plotted as a function of the rubber particle size at a constant amount of the rubber phase in Figure 2. The relationship between the impact strength and the rubber particle size is represented by a bell-shaped curve, *i.e.* the toughness has a maximum at an optimum rubber particle size. This is typical for the toughening of brittle polymers such as polystyrene and styrene-acrylonitrile copolymers^{12,13,17}. As can be seen in Figure 2, the optimum particle size is around $0.25 \mu\text{m}$ irrespective of the rubber phase fraction. These results are similar to the reported values¹⁵.

The impact strength data in Figure 2, with some additional data, are replotted as a function of the rubber

phase content in Figure 3. The impact strength increases up to a certain level of rubber phase content and decreases above that level. The blends containing $0.8 \mu\text{m}$ particles clearly show a maximum toughness around 12 wt.% of rubber phase fraction, and further inclusion of the rubber particles gives rise to a decrease in toughness. Lovell *et al.* have reported similar results for PMMA blends containing $0.8 \mu\text{m}$ rubber particles⁸. In the case of blends containing $0.25 \mu\text{m}$ particles, a very gentle hill-top occurs around a 10 wt.% rubber phase content and the decrease of the impact strength is not so significant with further inclusion of rubber particles. However, for most of the particle sizes, the toughness decreases over a certain rubber phase content.

The decrease of toughness above a certain rubber phase content is related to the decrease of the modulus and yield stress with increasing rubber phase content. If blends have a low modulus and low yield stress, the stress cannot be transferred far from the crack tip. Thus, the crack propagates without a large deformation of the matrix component near the crack tip. This results in a decrease of the stress whitening zone and the toughness.

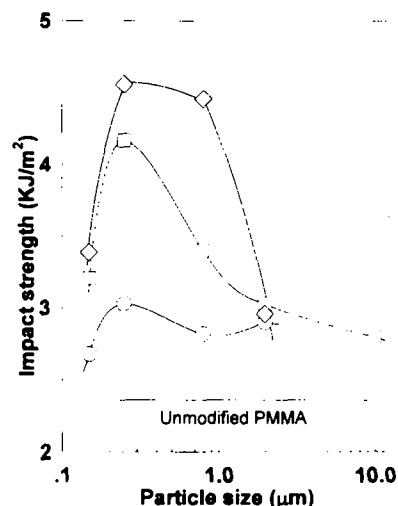


Figure 2 Impact strength as a function of rubber particle size. Rubber phase contents: \circ , 4 wt.%; \square , 8 wt.%; \diamond , 12 wt.%; --- , unmodified PMMA.

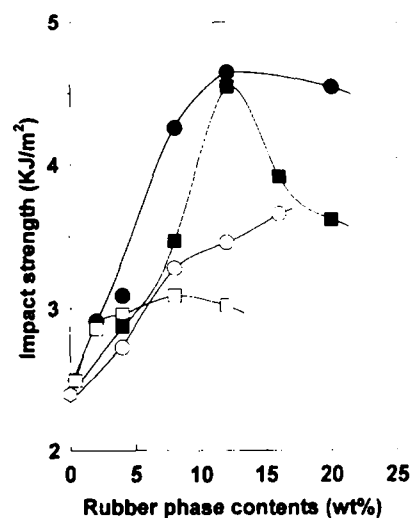


Figure 3 Impact strength as a function of rubber phase content. Rubber particle size: \circ , $0.15 \mu\text{m}$; \bullet , $0.25 \mu\text{m}$; \blacksquare , $0.8 \mu\text{m}$; \square , $2 \mu\text{m}$; ∇ , neat PMMA.

Effect of test method

The fracture toughness (K_{IC}) of the blends containing 2 μm particles and 0.25 μm particles (coded 2 μm blend and 0.25 μm blend, respectively) was measured by the three-point bending test (Figure 4) and the results are compared with those of the impact test (Figures 2 and 3). By the impact test, only a slight improvement of the impact strength was achieved for 2 μm blends (Figures 2 and 3). However, for the K_{IC} values determined by the three-point bending test, even the 2 μm blends show a significantly higher fracture toughness than neat PMMA. The 0.25 μm blends still show a toughness superior to that of the 2 μm blends (Figure 4). These results clearly reveal that the different fracture test methods, *i.e.* the three-point bending test and the impact test, give a different toughening behaviour for the same specimen. This may be due to the difference in the deformation mode of the matrix polymer around the rubber particles.

Microscopy examination

In order to obtain some insights into the deformation behaviour of the matrix polymer surrounding the rubber particles, the fracture subsurface of the deformed region was

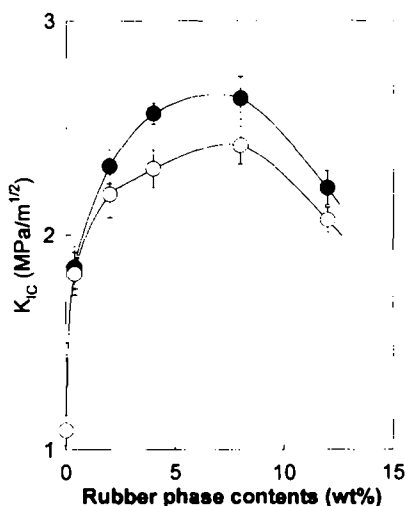


Figure 4 Fracture toughness (K_{IC}) as a function of rubber phase content. Rubber particle size: ●, 0.25 μm ; ○, 2 μm

examined. The deformed region beneath the fracture surface was sectioned, ground and polished to a thickness of about 20 μm . These sections were made normal to the fracture surface but parallel to the cracking direction. The thin section was then observed with the transmission optical microscope (TOM) under a bright field.

The TOM micrographs of the fracture subsurfaces obtained by both the three-point bending and the impact tests for the 2 μm 8 blend (8 represents the weight fraction of the rubber phase) are shown in Figure 5. The specimen subjected to the three-point bending test shows extensive deformation bands between the rubber particles (Figure 5a). The deformation band appears to be composed of numerous fine damage lines. In contrast, visible deformation of the matrix phase cannot be observed in the micrograph of the impact test specimen (Figure 5b). Only cavitation of the rubber particles is observed.

In order to examine the deformed region neighbouring a crack tip, the double-notched four-point bending test was performed^{18,19} and the deformed region around the unfractured notch tip of the specimen was examined by TEM. A TEM micrograph of the 2 μm 8 blend is shown in Figure 6. In the micrograph, a crack propagates from the left to the right. Rubber particles and craze-like damage lines are clearly observed. The crack appears as thick dark lines due to the deposition of O_5O_4 . PMMA and PBA do not have unsaturated chemical groups. However, partial staining of the PBA phase can occur due to selective absorption of O_5O_4 and subsequent reduction of O_5O_4 to O_5O_2 by the impurities in the polymers and in the air²⁰. Selective absorption possibly occurred because of a relatively large amount of free volume of PBA at room temperature. Therefore, the PBA rubber particles look darker in the micrograph. Crazes and voids are also clearly observed as dark images.

The observed craze lines look very fine and are initiated at the rubber particles. The deformation bands observed by TOM in the three-point bending specimens (Figure 5a) seem to be composed of large numbers of these fine craze lines. Figure 7 is a higher magnification of the micrograph of Figure 6. Numerous very fine craze lines are clearly observed throughout the PMMA matrix. The craze lines seem to be composed of many small voids. Besides the craze lines, very small voids of maximum size 200 nm are

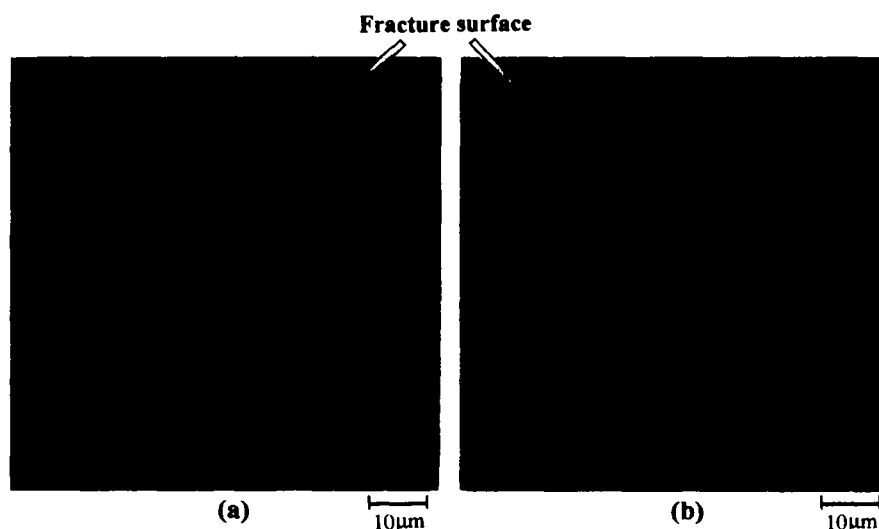


Figure 5 Optical micrographs of fracture subsurface for the blends containing 8 wt.% of 2 μm rubber particles: (a) three-point bending test; (b) impact test

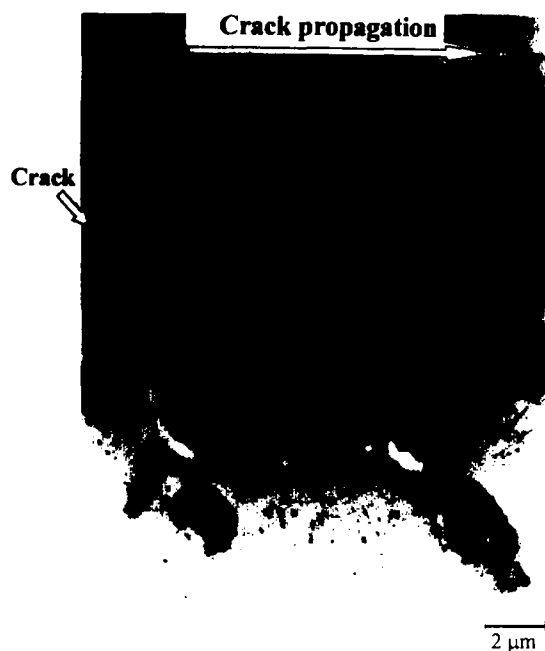


Figure 6 TEM micrograph of the deformed region of the double-notched four-point bending test specimen around the crack tip. The specimen contained 8 wt.% of 2 μm rubber particles



Figure 8 TEM micrograph of the deformed region around the crack tip for the double-notched four-point bending test specimen. The specimen contained 8 wt.% of 0.25 μm rubber particles



Figure 7 Higher magnification micrograph of *Figure 6*

also observed. The sizes of these small voids are considerably smaller in comparison with the size of the incorporated rubber particles. In the TEM micrograph of the blends containing small-size particles, *i.e.* 0.25 μm 8 blends, craze lines can also be clearly observed (*Figure 8*). These TEM micrographs clearly demonstrate that the deformation mechanism of rubber-toughened PMMA by the three-point bending test is mainly crazing.

TOM micrographs of the deformation zone of the 0.25 μm 8 blend and the 2 μm 8 blend fractured by impact test are shown in *Figure 9a* and *9b*, respectively. Both of the blends show considerable stress whitening near the notch tip and fracture surface. The sizes of the stress whitening zone

for both blends are comparable. However, the impact strength of the 2 μm blends is much lower than that of the 0.25 μm blends, as already seen in *Figure 3*.

In order to obtain some insight into the cause of the stress whitening, the deformation zone near the notch tip was examined by TEM. Schematic diagrams of the deformation region for the 0.25 μm 8 blend and the 2 μm 8 blend are shown in *Figure 10a* and *10b*, respectively. Also, transmission electron micrographs of some specific parts of the deformation region represented schematically in *Figure 10* are shown in *Figure 11a–11c*. For the 0.25 μm 8 blends, a few craze lines can be seen in the region very close to the notch tip (*Figure 11a*). In the deformation zone, which is several tens of micrometres away from the notch tip of the same specimen, there are cavitated rubber particles but only a few craze lines (*Figure 11b*). On the other hand, in the case of the 2 μm 8 blends, cavitation of the rubber particles can be observed but no craze lines are observed (*Figure 11c*). However, the number of craze lines of the 0.25 μm 8 blends produced by the impact test as shown in *Figure 11a* and *11b* is too small for them to absorb much energy during the fracture process. Therefore, it is speculated that much of the impact energy was absorbed by the shear deformation process. Thus, deformation might occur via a mixed mode of crazing and shear yielding. The deformation mechanisms will be discussed in detail in Section 4.

SEM micrographs of the fracture surface of the specimen containing 8 wt.% of 2 μm particles after the three-point bending test and the impact test are shown in *Figure 12a* and *12b*, respectively. The small voids observed in the TEM micrographs (*Figure 7*) are also observed as small holes in the SEM micrograph of the fracture surface (*Figure 12*). On the fracture surface obtained by the three-point bending test (*Figure 12a*), a very rough structure can be seen, which implies that massive deformation of the PMMA matrix occurred. Moreover, it looks as though the rubber particles have not adhered well to the PMMA matrix, *i.e.* the rubber

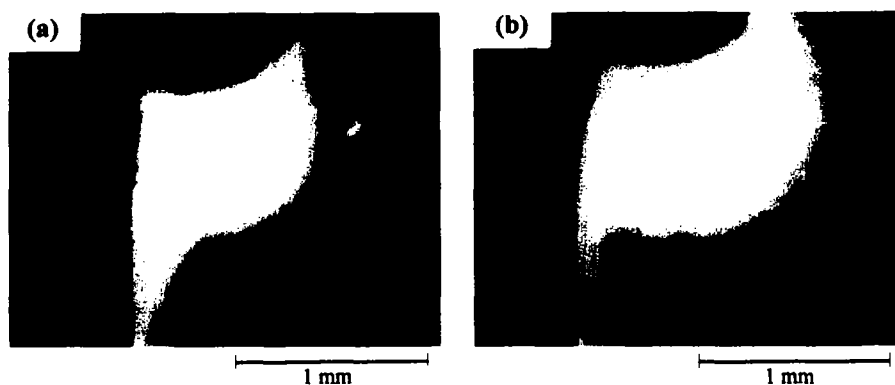


Figure 9 Optical micrographs of the deformed region of the impact test specimen perpendicular to the fracture surface: blends containing 8 wt.% of (a) 0.25 μm rubber particles, and (b) 2 μm rubber particles

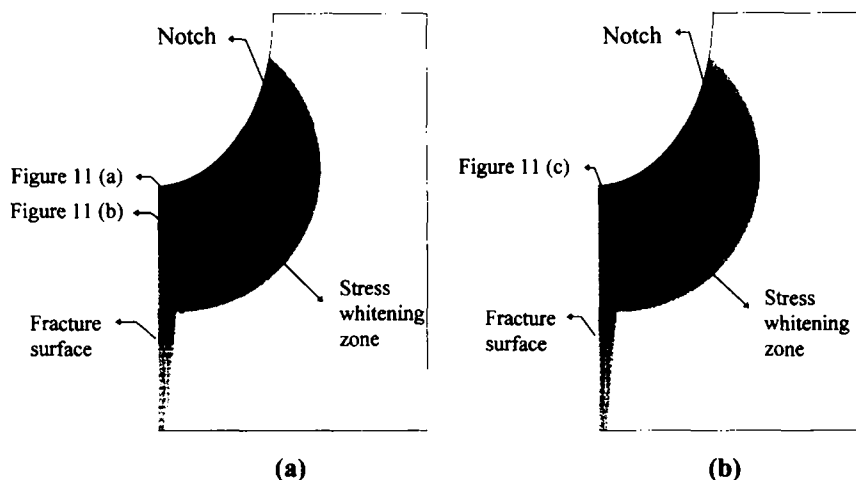


Figure 10 Schematic drawing of a deformation region of an impact test specimen perpendicular to the fracture surface: (a) blends containing 8 wt.% of (a) 0.25 μm rubber particles, and (b) 2 μm rubber particles

particles are detached from the PMMA matrix and only some part of the rubber particles is connected to the matrix by fine fibrils. In contrast, for the impact test specimen (Figure 12b), the interface is fairly well adhered. The different interfacial structure after the fracture test reveals that massive plastic deformation occurred in the PMMA matrix for the three-point bending test rather than for the impact test for the specimen containing 2 μm particles. This result of the microscopy observations is consistent with the results of the fracture test, *i.e.* a significant enhancement of the fracture toughness for the three-point bending test, but only a small increase for the impact test.

For the specimen containing fairly small-size particles, such as 0.25 μm particles, the fracture surface of the three-point bending test specimen (Figure 13a and 13b) looks very similar to that of the 2 μm blends. A very rough structure all over the fracture surface, large voids at the interface and fine fibrils connecting the rubber particles and the matrix are clearly observed in the higher magnification micrograph (Figure 13b), which indicates that massive plastic deformation had taken place.

DISCUSSION

As already shown in the experimental results in Section 3, the toughening behaviour of rubber-toughened PMMA is significantly influenced by the test method, *i.e.* the three-point bending test or the impact test. In order to explain the

different toughening behaviour of 2 μm blends for the three-point bending test and the impact test, as already shown in Figures 2–4, the deformation and the fracture mode of the matrix PMMA around the particles and the notch tip of the specimen should be considered.

As already seen in Figures 12 and 13, SEM micrographs of the fracture surfaces show a very rough structure, which implies that massive plastic deformation occurred. However, the SEM micrographs do not indicate the type of plastic deformation. In this sense, the TEM micrographs (Figures 6–8) clearly reveal that crazing took place during crack propagation in rubber-toughened PMMA by the three-point bending test.

The deformation mechanism of unmodified PMMA is known to be crazing^{13,14}. However, many contradicting results have been reported in the literature with regard to the deformation mechanism of rubber-toughened PMMA. Bucknall *et al.* could not observe any change in the volumetric strain during a creep test of rubber-toughened PMMA², and Hooley *et al.* found that the increase of volumetric strain for rubber-toughened PMMA is smaller than that for neat PMMA during tensile testing¹. Thus, they proposed that the principal deformation mechanism of rubber-toughened PMMA is shear yielding. Milios *et al.* have studied the crack propagation behaviour under high speed testing and they have concluded that rubber-toughened PMMA is mainly deformed by the shear yielding process⁴. All these results demonstrate that

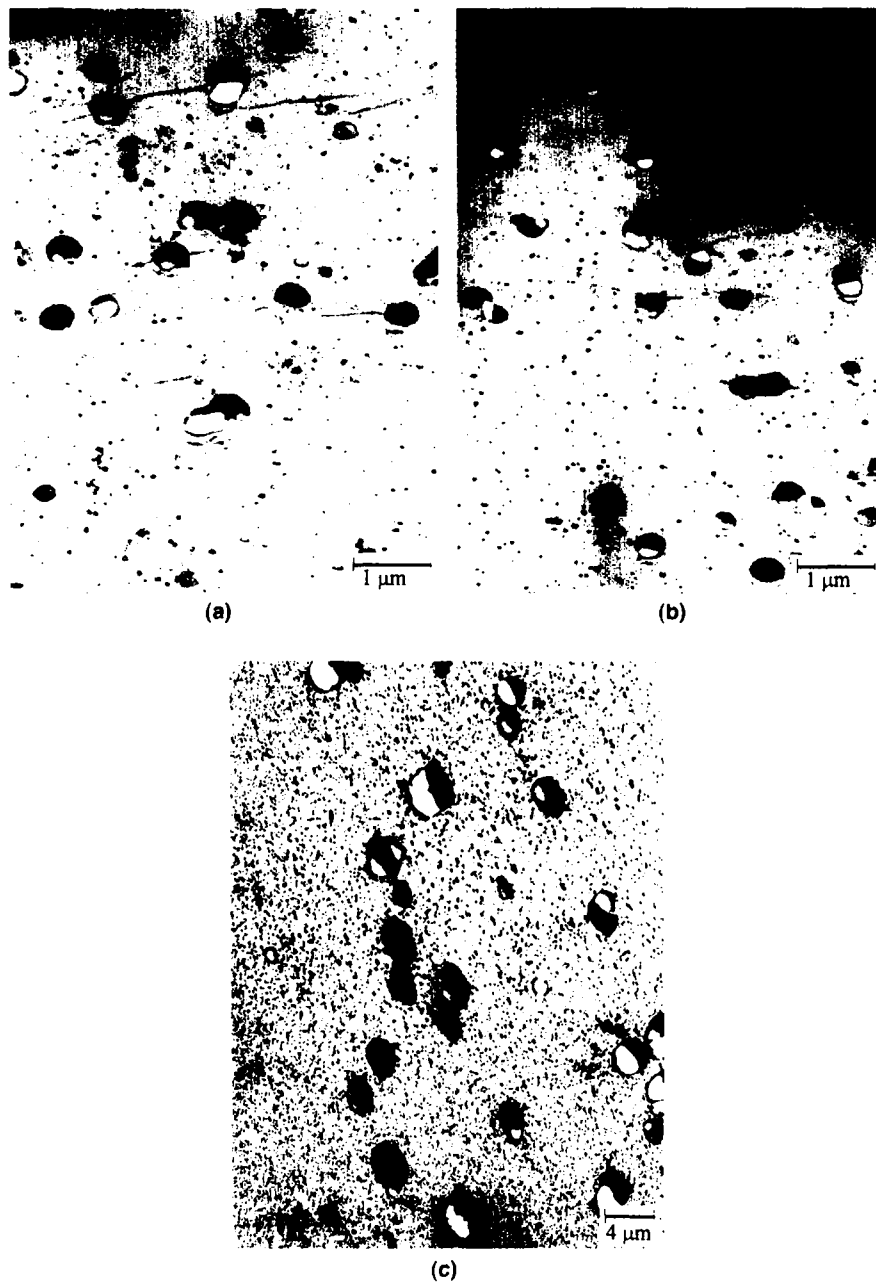


Figure 11 TEM micrographs of the deformed region around the crack tip: (a), (b), and (c) are shown in the schematic drawing of *Figure 10*. (a) Very close to the notch tip of the blend containing 8 wt.% of 0.25 μm rubber particles; (b) several tens of micrometres away from the notch tip of the blend containing 8 wt.% of 0.25 μm rubber particles; (c) very close to the notch tip of the blend containing 8 wt.% of 0.25 μm rubber particles

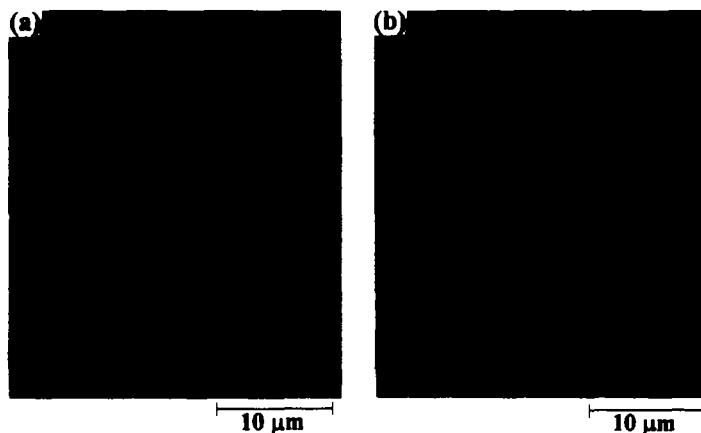


Figure 12 SEM micrographs of the fracture surface for the blend containing 8 wt.% of 2 μm rubber particles: (a) three-point bending test; (b) impact test

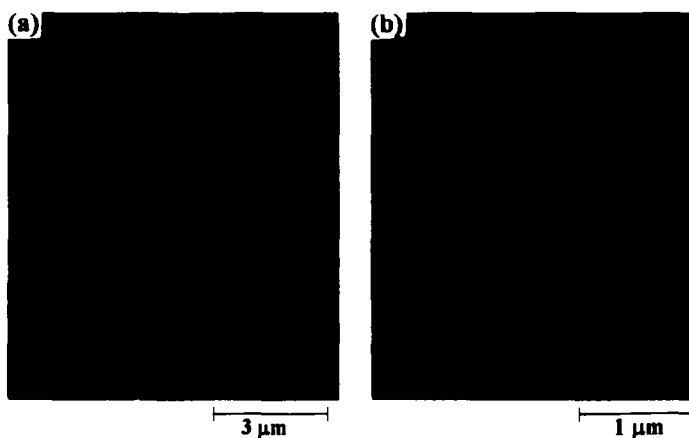


Figure 13 (a) SEM micrographs of the fracture surface for the blend containing 8 wt% of 0.25 μm rubber particles by the three-point bending test; (b) higher magnification of (a)

rubber-toughened PMMA is deformed by shear yielding during tensile tests.

On the other hand, Shah reported that crazing could occur even in rubber-toughened PMMA in the impact test when the modifier loading was low, but he did not find any evidence of crazing when the modifier content was higher than 20 wt.%³. Pavan and Mercante found that the craze stress of the PMMA around single rubber particle inclusion was lower than the yield stress of unmodified PMMA irrespective of the plane strain or plane stress conditions, which suggested that crazing was more favourable than shear yielding for rubber-toughened PMMA⁶. Recently, Lovell *et al.* have found multiple crazing in rubber-toughened PMMA generated during the double-notched four-point bending test and the double-notched Charpy impact test⁹.

In our experimental results, crazing is observed during the three-point bending test. On the other hand, the deformation occurred in a mixed mode of crazing and shear yielding for the impact test. The different deformation mechanism due to the fracture test method is possible related to the disentanglement behaviour of the PMMA chain in the deformation region. For crazing, molecular chains have to be disentangled during loading. Therefore, crazing of rubber-toughened PMMA can occur below some critical strain rate and at a high tri-axial stress state for rubber-toughened PMMA. These conditions may be satisfied at the notch tip by the three-point bending test. Under other test conditions, such as impact, tensile or creep testing, shear yielding is preferred to crazing.

In the three-point bending test, there is time enough for the PMMA chain to be disentangled; therefore, deformation can occur by crazing. On the other hand, in the case of the impact test, the test speed is much higher than that of the three-point bending test by approximately five orders (the test speed of the three-point bending test is 1.28 mm min⁻¹ and that of the impact test is 335 cm s⁻¹). The time is not long enough for disentanglement of the PMMA chain. Therefore, the deformation occurred in the mixed deformation mode but the main deformation mechanism is shear yielding.

In the case of the impact test, it is suggested that the deformation mechanism of rubber-toughened PMMA is mainly shear yielding induced by cavitation of the rubber particles. However, unfortunately, no direct experimental evidence of shear yielding was obtained due to the experimental difficulties.

Thus, it is inferred that the impact strength of rubber-toughened PMMA is related to the shear yielding ability of the matrix, which is governed by the ease of cavitation of the rubber particles. Lazzeri and Bucknall investigated the cavitation behaviour of rubber particles and the subsequent yield behaviour induced by particle cavitation²¹. They proposed that particles with diameters less than 0.13 μm could not be cavitated. For shear yielding, the stress field in the matrix should be turned into plane stress from plane strain, resulting from particle cavitation. Therefore, smaller particles less than a critical size cannot play the role of toughening agent. Gaymans and co-workers also reported that the impact strength is related to the rubber particle cavitation ability for nylon/rubber blends²². They investigated the toughening behaviour of nylon/rubber blends using various rubber particles, and suggested that rubber particles with a low modulus and low Poisson's ratio may be easily cavitated and induce higher toughness. In our studies, it seemed that the rubber particles in the 0.15 μm blends were too small to be cavitated and the toughness, therefore, was not improved much, as was already shown in Figure 2.

In the 2 μm blends, the rubber particles could easily be cavitated, as already seen in Figure 5b, but the interparticle distance was too large to alter the state of the stress field. Therefore, the toughness was not much improved. As a result, the impact toughness showed a maximum value at a rubber particle size of 0.25 μm .

CONCLUSIONS

The present study of the toughening behaviour of rubber-toughened PMMA enables us to recognize the effect of the particle size in different fracture tests. In the case of the impact test, a maximum impact strength was obtained around a rubber particle size of 0.25 μm , regardless of the rubber phase contents. The blends containing 0.15 or 2 μm particles showed only a slight improvement in impact strength. On the other hand, by the three-point bending test, the blends containing the 2 μm particles showed quite a large improvement in fracture toughness, K_{IC} , values. These conflicting results for the 2 μm blends in the different test methods suggest that the deformation mechanism of rubber-toughened PMMA is governed by the strain rate and the loading behaviour. It was also shown that the toughening mechanism of rubber toughened PMMA is mainly multiple crazing in the three-point bending test, whereas shear

yielding induced by particle cavitation is predominant in the impact test.

ACKNOWLEDGEMENTS

This work was supported in part by a research grant from the Ministry of Education Research Funds for Advanced Materials, 1996. The research grants from the Centre for Advanced Functional Polymers and the School of Environmental Engineering of Pohang University of Science and Technology are also gratefully acknowledged.

REFERENCES

1. Hooley, C. -J., Moor, D. R., Whale, M. and Williams, M. J., *Plast. Rubber Proc. Appl.*, 1981, **1**, 345.
2. Bucknall, C. B., Partridge, J. K. and Ward, M. V., *J. Mater. Sci.*, 1984, **19**, 2064.
3. Shah, J., *J. Mater. Sci.*, 1988, **23**, 3623.
4. Milios, J., Papanicolau, G. C. and Young, R. J., *Plast. Rubber Proc. Appl.*, 1989, **11**, 37.
5. Mauzac, O. and Schirrer, R., *J. Mater. Sci.*, 1990, **25**, 5125.
6. Pavan, A. and Mercante, L., *Makromol. Chem. Makromol. Symp.*, 1991, **48/49**, 221.
7. Gloaguen, J. M., Heim, P., Gaillard, P. and Lefebvre, J. M., *Polymer*, 1992, **33**, 4747.
8. Lovell, P. A., McDonald, J., Saunders, D. E. J., Sherratt, M. N. and Young, R. J., *Plast. Rubber Comp. Proc. Appl.*, 1991, **16**, 37.
9. Lovell, P. A., Ryan, A. J., Sherratt, M. N. and Young, R. J., *Polym. Mater. Sci. Eng.*, 1994, **70**, 155.
10. Cho, K., Yang, J. and Park, C. E., *Polymer*, 1997, **38**, 5161.
11. Cho, K., *Polymer (Korea)*, 1993, **17**, 176.
12. Bucknall, C. B., *Toughened Plastics*, Applied Science, London, 1977.
13. Kinloch, A. J. and Young, R. J., *Fracture Behavior of Polymers*, Applied Science, 1983.
14. Michler, G. H., *J. Mater. Sci.*, 1990, **25**, 2321.
15. Wrotecki, C., Heim, P. and Gaillard, P., *Polym. Eng. Sci.*, 1991, **31**, 213.
16. Cook, D. G., Rudin, A. and Plumtree, A., *J. Appl. Polym. Sci.*, 1992, **46**, 1387.
17. Cook, D. G., Rudin, A. and Plumtree, A., *J. Appl. Polym. Sci.*, 1993, **48**, 75.
18. Pearson, R. A. and Yee, A. F., *J. Mater. Sci.*, 1991, **26**, 3828.
19. Holik, A. S., Kambour, R. P., Hobbs, S. Y. and Fink, D. G., *Microstruct. Sci.*, 1979, **7**, 357.
20. Sawyer, L. C. and Grubb, D. T., *Polymer Microscopy*, Chapman and Hall, New York, 1987.
21. Lazzeri, A. and Bucknall, C. B., *J. Mater. Sci.*, 1993, **28**, 6799.
22. Borggreve, R. J., Gaymans, R. J. and Eichenwald, H. M., *Polymer*, 1989, **30**, 78.